Electronic States in Vitreous Selenium*

J. L. HARTKE AND PAUL J. REGENSBURGER†
Research and Engineering Center, Xerox Corporation, Webster, New York
(Received 12 March 1965)

The quantum efficiency for photoproduction of electrons and holes in vitreous selenium has been measured at room temperature for photon energies between 2.0 and 3.1 eV. Electrons and holes are found to be created in pairs with energy-dependent quantum efficiencies varying from an assumed value of unity near 3 eV to 2×10^{-4} at 2 eV. A general relation between quantum efficiencies and optical properties is developed which, along with conventional band theory, explains the optical properties of vitreous selenium in terms of two different types of optical transitions. One type, assumed to have unit quantum efficiency, is interpreted in terms of direct allowed transitions between valence and conduction bands which are separated by an energy gap of 2.53 eV. Energetically shallow tails at the band edges resemble shallow traps which have been observed in transport measurements. The other type of optical transition, assumed to occur with zero quantum efficiency, is attributed to intrinsic exciton absorption. The shape of this absorption band closely resembles that expected for the two-lattice-mode model of phonon-assisted transitions and accounts for the absorption edge of vitreous selenium, which obeys Urbach's empirical rule. The observed generation of mobile electrons alone at photon energies less than 2 eV is assigned to transitions from filled states just below the Fermi level to the conduction band. Several authors have proposed such a model to account for the absorption edge, but the small observed quantum efficiency for these transitions suggests that they contribute very little to the total absorption.

I. INTRODUCTION

THE presence of short-range atomic order in vitreous (amorphous) selenium has encouraged the use of solid-state band theory in interpreting the results of electronic-transport measurements.[1–5] Although these measurements have identified the presence of mobile carriers of both charge signs as well as several trapping levels in the band gap, the results are relatively insensitive to the actual band structure. Indeed, if properly motivated, one could probably explain the results without invoking the band model. The optical properties of a semiconductor are quite sensitive to the band structure, but extensive optical measurements[6–14] in selenium have failed to produce any definitive interpretations. Although the accurately measured and reproducible optical-absorption coefficient, shown in Fig. 1, has a long-wavelength edge and attains a high value which persists over a considerable energy range, characteristic of interband transitions, the width in energy of the absorption edge is far in excess of that expected for strong interband transitions. The absorption edge actually increases exponentially in photon energy and appears to obey[15] Urbach's empirical rule[16]; the mechanism responsible for this rule has not been firmly established.

Measurements[2,8,17–19] of the spectral response of photoconductivity in vitreous selenium partially support the band model since the number of free carriers generated per absorbed photon (quantum efficiency) is near unity[17,20] at short wavelengths. However, as shown[21] in Fig. 1, the quantum efficiency at long wavelengths is small, even in regions of strong absorption. The optical and photoconductive properties suggest that absorption occurs by interband transitions at high photon energies and by some other mechanism near the absorption edge. Dresner[2] discussed a number of models for the edge but found none to be wholly satisfactory, while Lanyon[5] quantitatively fitted the absorption edge by attributing it to transitions from filled states lying just below the Fermi level to the conduction band. All models presuppose distinctly different quantum efficiencies for electrons and holes near the absorption edge. Previous workers[2,8,17–19] have not looked for this difference.

The purpose of this work was to separately measure

* Preliminary results have been presented to the American Physical Society [Bull. Am. Phys. Soc. 8, 210 (1963)].

† Present address: University of Rochester, Rochester, New York.

[1] W. E. Spear, Proc. Phys. Soc. (London) **B70**, 669 (1957); **B76**, 826 (1960).
[2] J. Dresner, J. Chem. Phys. **35**, 1628 (1961).
[3] H. P. D. Lanyon and W. E. Spear, Proc. Phys. Soc. (London) **76**, 1157 (1961).
[4] J. L. Hartke, Phys. Rev. **125**, 1177 (1962).
[5] H. P. D. Lanyon, Phys. Rev. **130**, 134 (1963).
[6] H. A. Gebbie and E. W. Saker, Proc. Phys. Soc. (London) **B64**, 360 (1951).
[7] J. J. Dowd, Proc. Phys. Soc. (London) **B64**, 783 (1951).
[8] M. A. Gilleo, J. Chem. Phys. **19**, 1291 (1951).
[9] J. Stuke, Z. Physik **134**, 194 (1953).
[10] C. Hilsum, Proc. Phys. Soc. (London) **B69**, 506 (1956).
[11] W. F. Koehler, F. K. Odenkrantz, and W. C. White, J. Opt. Soc. Am. **49**, 109 (1959).
[12] R. S. Caldwell and H. Y. Fan, Phys. Rev. **114**, 664 (1959).
[13] H. Gobrecht and A. Tausend, Z. Physik **161**, 205 (1961).
[14] W. Kamprath, Ann. Physik **9**, 382 (1962).
[15] It has not been firmly established that the temperature dependence of the absorption edge follows Urbach's rule since low-temperature measurements (Ref. 8) cover only the low absorptivity range and are uncorrected for reflection losses.
[16] R. S. Knox, *Solid State Physics, Supp. 5*, edited by F. Seitz and D. Turnbull (Academic Press Inc., New York, 1963), p. 154.
[17] P. K. Weimer and A. D. Cope, RCA Rev. **12**, 314 (1951).
[18] P. H. Keck, J. Opt. Soc. Am. **42**, 221 (1952).
[19] R. A. Fotland, J. Appl. Phys. **31**, 1558 (1960).
[20] H. T. Li and P. J. Regensburger, J. Appl. Phys. **34**, 1730 (1963); P. J. Regensburger, J. Appl. Phys. **35**, 1863 (1964).
[21] Relative measurements (Refs. 2, 8, 18, 19) were normalized to unity at 3.1 eV and results (Refs. 8, 17, 18) based on conditions of constant incident energy were converted to constant photon flux.

electron and hole quantum efficiencies in the region of strong absorption, to combine the results with the known optical properties, and to interpret the composite in a manner which gives a better understanding of the electronic energy structure of this noncrystalline solid.

II. THEORY

The relationship between observed quantum efficiencies and optical properties of a photoconductor is best approached by first summarizing the optical parameters which are commonly used and their relationships to the physical phenomenon of absorption. One parameter, a complex number, is sufficient to characterize the optical properties of a medium. The real part of the parameter generally relates the energy density or flux velocity in the medium to that in vacuum, while the imaginary part is a measure of the dissipation rate of electromagnetic energy density in the medium. One form of the complex parameter may be the index of refraction, $N=n-ik$, where n is the ordinary index and k is the extinction coefficient. The absorption coefficient is related to k by the expression $c\alpha=4\pi\nu k$, with c and ν, respectively, the velocity in vacuum and the frequency of the light. Another possible complex parameter is the dielectric constant $\epsilon=\epsilon_1-i\epsilon_2$ which is comprised of the real and imaginary part ϵ_1 and ϵ_2. Using the identity $\epsilon=N^2$, the following relations may be established:

$$\begin{aligned}\epsilon_1&=n^2-k^2,\\ \epsilon_2&=2nk=(2\pi\nu)^{-1}cn\alpha.\end{aligned}\tag{1}$$

Although the value at a given wavelength of any one complex parameter is sufficient to determine all others at that wavelength, it is necessary to know only one real or one imaginary part over a wide frequency range. All other parameters may then be obtained through use of the Kramers-Kronig dispersion relations,[22] of which two examples follow:

$$\epsilon_1(\nu_0)=1+\frac{2}{\pi}\int_0^\infty\frac{\epsilon_2(\nu)\nu d\nu}{\nu^2-\nu_0^2},\tag{2a}$$

$$\epsilon_2(\nu_0)=-\frac{2\nu_0}{\pi}\int_0^\infty\frac{\epsilon_1(\nu)d\nu}{\nu^2-\nu_0^2}.\tag{2b}$$

Having established that only one real or imaginary parameter is necessary, it will now be shown that one particular optical parameter is most useful when several different absorption mechanisms contribute to the optical properties of the solid. This parameter must be a sum of like parameters, each of which represents one absorption mechanism and is independent of all others.

A brief survey of the well-established theory of optical absorption[23] will show that the total optical-absorption coefficient arising from several independent absorption mechanisms may always be written as $\alpha=n^{-1}\sum_j n_j\alpha_j$, enabling the most useful optical parameter to be readily selected. Classical theory for metals gives the absorption coefficient as

$$\alpha=(4\pi/nc)\textstyle\sum_j\sigma_j,\tag{3}$$

where the total electrical conductivity σ is a sum of contributions from independent conduction processes. In the classical Lorentz model, a dispersive and absorbing medium is characterized by a collection of uncoupled harmonic oscillators, each having mass m, effective charge $ef_j^{1/2}$, natural frequency ν_{0j}, damping constant $2\pi\gamma_j$, and density N. The absorption coefficient for this model is

$$\alpha=(2Ne^2/mnc)\textstyle\sum_j(f_j\gamma_j\nu^2/(\nu_{0j}^2-\nu^2)^2-\gamma_j^2\nu^2).\tag{4}$$

Semiclassical theory for optical absorption, which employs first-order time-dependent perturbation theory and treats the radiation field semiclassically, yields the following absorption coefficient:

$$\alpha=(h\nu/I)\textstyle\sum_j N_jw_j=(\pi e^2h/mnc\nu)\sum_j N_j\nu_jf_j\delta(\nu_j-\nu).\tag{5a}$$

The parameter I is the energy flux in the medium, N_j is the density of absorbing centers, w_j is the transition rate per absorbing center, and $h\nu_j$ is the energy separating the final and initial states. The oscillator strength f_j in Eq. (5a) is proportional to the square of the matrix element of the time-independent part of the perturbing Hamiltonian taken between final and initial states, and is defined as

$$f_j=(2/mh\nu_j)|\langle f_j|\exp(i\mathbf{q}\cdot\mathbf{r})\mathbf{a}\cdot\mathbf{p}|i_j\rangle|^2,\tag{6}$$

where $\mathbf{q}$ is the photon momentum, $\mathbf{a}$ is the unit polarization vector of the vector potential $\mathbf{a}A_0$, and $\mathbf{p}$ is the momentum operator. Having established through Eqs.

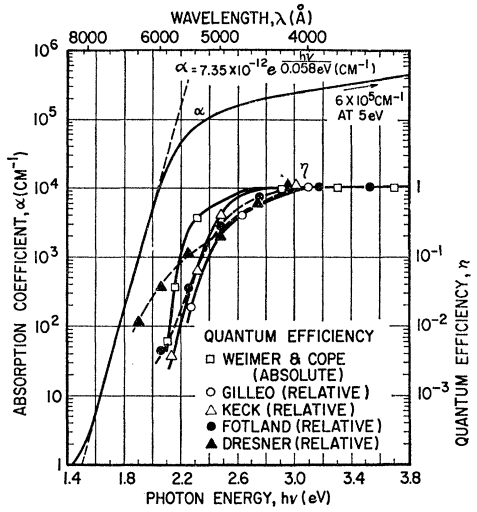

FIG. 1. Optical-absorption coefficient and quantum efficiencies for vitreous selenium at room temperature.

[22] T. S. Moss, *Optical Properties of Semi-Conductors* (Academic Press Inc., New York, 1959), Sec. 2.4 and Appendix B.

[23] For a review and additional references see Ref. 16, Sec. 8–9.

(3)–(6) the equality $n\alpha=\sum_j n_j\alpha_j$, it is apparent that, although neither the ordinary index n_j nor the absorption coefficient α_j is additive and independent, their product $n_j\alpha_j=2\pi\nu c^{-1}\epsilon_{2j}$ is additive[24] and is independent of all other absorption processes, showing that the imaginary part of the dielectric constant is the most useful optical parameter. This becomes clearer if Eq. (5a) is rewritten as

$$\epsilon_2\nu^2=\nu^2\sum_j\epsilon_{2j}=\frac{hc^2}{4\pi^2}\sum_j N_j\frac{w_j}{A_0^2}$$

$$=\frac{e^2h}{2m}\sum_j N_j\nu_j f_j\delta(\nu_j-\nu)\,, \qquad (5b)$$

from which one sees that ϵ_2 (or ϵ_{2j}) is directly related to the normalized transition rate w/A_0^2 (or w_j/A_0^2).

The observable quantum efficiency η of a photoconductor is defined as the number of mobile charge carriers generated by one absorbed photon. Defining C as the density of photogenerated mobile carriers of a given charge sign, N_q as the photon density, and using the identity $-\partial N_q/\partial t=\sum_j N_j w_j$, one obtains

$$\partial C/\partial t=-\eta(\partial N_q/\partial t)=\eta\sum_j N_j w_j=\sum_j\eta_j N_j w_j\,, \qquad (7)$$

where η_j is the quantum efficiency of the jth absorption mechanism. Upon substitution from Eq. (5b) of the relationship between ϵ_2 and the transition rate, Eq. (7) becomes

$$\eta\epsilon_2=\eta\sum_j\epsilon_{2j}=\sum_j\eta_j\epsilon_{2j}\,. \qquad (8)$$

This relation couples the optical and photoconductive properties of a material and will be used to resolve the various electronic states for vitreous selenium.

III. EXPERIMENTAL TECHNIQUE

Quantum efficiency relates only to the generation of mobile charge carriers while photoconductivity measurements observe the generation process as well as transport losses through recombination or trapping of the mobile carriers and the effects of reflectivity and transmission losses. Transient measurements of primary photoconductivity as a function of applied electric field have been used[25] to factor out the transport losses and thus to determine the true quantum efficiency. The same method was employed here and, in addition, fast pulse techniques were used for the light source and for the charge detector. Pulse techniques, which have been used[1,4] to measure drift mobilities in vitreous selenium, were advantageous here in that charge generation and charge transport were time resolved. This enabled the true bulk, or primary, photoresponse to be separated from surface photogeneration or from secondary photoeffects characterized by the injection of charge from electrodes.

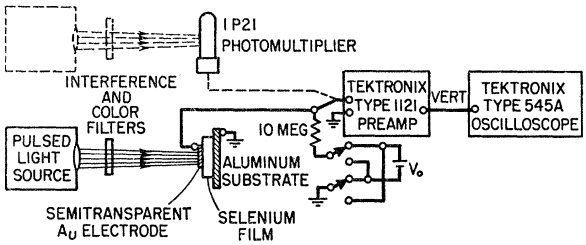

FIG. 2. Experimental arrangement used for the measurement of quantum efficiency.

The experimental arrangement is shown in Fig. 2. Fast, reproducible light pulses of 5-nsec half-width were generated by passing the output of a xenon-filled flashlamp through a Kerr cell shutter.[26] Very intense pulses of 1 μsec duration were obtained from the flashlamp alone. Nearly monoenergetic light pulses were derived using band-pass interference filters together with secondary color filters. A total of 11 filter assemblies covered the energy range between 2.0 and 3.1 eV. The spectral transmission curve of each filter was measured[27] to insure spectral purity; filter bandwidths were 0.03 to 0.11 eV. The light pulses were monitored using a photomultiplier whose spectral response had been measured, thereby obtaining the relative number of incident photons, N_q, for each filter assembly. The light pulses were absorbed in the photoconducting film to which a dc electric field was applied through blocking electrodes, and the resultant charge pulses were amplified and displayed on the cathode-ray tube of the oscilloscope. The charge detection system had a risetime of 25 nsec, much less than the risetime of a charge pulse, and had a noise level equivalent to 2×10^5 electronic charges.

The reciprocal of the optical absorption coefficient was always less than 10% of the sample thickness, enabling the drift of electrons and holes to be observed separately. The charge sign of the drifting carrier was selected by the polarity of the applied voltage. The amplitude of the charge pulse for each filter combination was measured over a wide range of applied voltage for both carriers, and the pulse amplitude, $v(E_0)$, was then fitted to a modified Hecht formula[20] of the form

$$v(E_0)=v_m(\mu E_0\tau_t/L)\exp(-\beta L/\mu E_0\tau_t)$$
$$\times[1-\exp(-L/\mu E_0\tau_t)]\,, \qquad (9)$$

where μ is the drift mobility, τ_t is the mean free drift

[24] The additivity of ϵ_{2j} is not generally valid if perturbations higher than first order are important and if more than one intermediate state contributes to the transition probability [J. J. Hopfield, Phys. Chem. Solids **22**, 63 (1961)]. The results of this section are valid if each component ϵ_{2j} is indexed only according to the initial and final state, sums over intermediate states being included in each component. This limitation is realistic since the presence or absence of photoconductivity depends only on the initial and final state.

[25] R. S. Van Heyningen and F. C. Brown, Phys. Rev. **111**, 462 (1958).

[26] STU-92 Pulse Modulated Light Source, Electro-Optical Instruments, Inc., Pasadena, California.

[27] Cary Model 14 Recording Spectrophotometer, Applied Physics Corporation, Monrovia, California.

time before "permanent" trapping, E_0 is the applied electric field, and L is the sample thickness. The factor $\exp(-\beta L/\mu E_0 \tau_t)$ approximates recombination losses near the thin absorption layer where excess carriers of both charge signs are present. One expects that $\beta \approx \tau_t(\tau_r \alpha L)^{-1}$, τ_r being the recombination lifetime. By fitting the pulse amplitudes measured for each charge carrier to Eq. (9), one obtains the constant v_m which is proportional only to the number of photogenerated carriers, all transport losses having been factored out. After correction for electrode transmission and reflection losses, the ratio v_m/N_q is proportional to the quantum efficiency.

Measurements between 2.3 and 3.1 eV were made using the Kerr cell shutter. The transmission of the nitrobenzene Kerr fluid was quite low for photon energies greater than 2.8 eV, resulting in a low signal-to-noise ratio and considerable experimental error in this region. High-intensity light pulses from the flashlamp alone were used in the 2.0 to 2.4 eV region where the quantum efficiency was small. The region of overlap from 2.3 to 2.4 eV permitted a smooth fit to be made between the results obtained using the two different light sources.

IV. SAMPLE PREPARATION AND SELECTION

All samples were prepared by evaporating high-purity selenium onto anodized aluminum substrates which were held at 50°C during the evaporation. Selenium film thicknesses were between 16 and 32 μ. The oxide layer on the aluminum substrate served as one blocking layer and a thin ($\approx$1000 Å) layer of polyvinyl chloride (PVC) was dip-coated over the selenium film to form the other blocking layer. A gold layer, 30 to 200 Å thick, was evaporated on top of the PVC layer and served as the semitransparent electrode.

To insure that the experimental results represented only primary bulk photoresponse, samples were selected which met two requirements. The first requirement was that the blocking layers must prevent charge from entering or leaving the sample during the time of measurement, and fulfillment of this requirement was evidenced by the observation of charge pulses which had sharp corners at the charge generation and collection times and which showed negligible photocurrents after the collection (transit) time. The second requirement was that surface photogeneration of mobile carriers (e.g., from surface states) must be absent. This requirement was tested by observing the photoresponse generated by penetrating, or uniformly absorbed, light pulses, thereby obtaining a spatially uniform distribution of charge carriers characteristic of the true bulk photogeneration in contrast to the nonuniform distribution expected of surface photogeneration. Examination of the magnitude and time dependence of the photoresponse for equal applied voltages of opposite polarity then enabled spurious surface effects to be identified. The sample was illuminated through a 50-μ-thick filter of vitreous selenium, thereby obtaining incident photons whose energies were less than 1.9 eV and which were absorbed uniformly in the sample. The amplitude and shape of the resulting charge pulses were independent of the polarity of the applied voltage; only the sign of the pulse reversed as polarity was reversed, showing that photoexcitation occurred only in the bulk. It was assumed that the absence of surface photogeneration for photon energies less than 1.9 eV also indicated that surface effects were absent in the 2.0- to 3.1-eV range since the threshold energy for surface excitation is expected to be less than that for bulk excitation. By using color filters in addition to the selenium filter, the long-wavelength bulk photoresponse was found to be in the 1.2- to 1.85-eV range. The quantum efficiency in this energy region was much less than 10^{-3} while the rise times of the charge pulses were characteristic of electrons alone. Hole drift mobility at room temperature is about 20 times that of electrons,[1,4] and fast hole pulses would have been readily distinguishable if mobile holes had been present.

Other samples were prepared using NESA-coated glass substrates which also provided the semitransparent electrode. Charge pulses generated by penetrating light were also characteristic of electrons alone, but the pulse amplitude observed with a negative illuminated electrode was several times larger than for the case of opposite polarity. This asymmetry indicated that more electrons were photoexcited at the NESA-selenium interface than were generated in the bulk. The photoresponse of these samples for photon energies between 2.0 and 2.6 eV was greater than the response of samples which did meet all selection requirements, suggesting that differences between previous workers' results might be caused by spurious surface photoexcitation.

V. EXPERIMENTAL RESULTS

Room-temperature photoresponse was measured separately for electrons and holes at eleven photon energies using four selected samples. The relative number of photoexcited carriers, v_m, was determined using the modified Hecht formula of Eq. (9); typical results are shown in Fig. 3. High-field points were usually above the theoretical curve, presumably because of a slight amount of carrier injection through the blocking electrodes. Within experimental error, electrons and holes were always generated as pairs. Carrier ranges, or $\mu\tau_t$ values, were between 4×10^{-8} and 1×10^{-7} cm^2/V and were in good agreement with published values.[4,20] Drift mobilities were also measured and were the same as published values.[1,4]

The values obtained at field saturation for v_m were corrected for the wavelength dependence of electrode transmission and reflection losses; these losses were determined separately for each sample. The dependences

on photon energy of the corrected saturation values obtained from each of the four samples were statistically combined in each of the two energy regions corresponding to the different light sources. These values were then divided by N_q, the relative number of incident photons at a given photon energy for the appropriate light source, and the results from the two energy ranges were matched in the 2.3 to 2.4 eV overlap region. The resulting data points are shown in Fig. 4 along with the best fit to the points, represented by the dashed curve. This curve was corrected for the finite bandwidth of the optical filters, giving the solid curve of Fig. 4 which is the relative quantum efficiency of vitreous selenium at room temperature. The plateau in the response between 2.8 and 3.1 eV was assumed to represent a quantum efficiency of unity, thereby converting the relative results to absolute values. The validity of this assumption rests upon published quantum efficiency values[17,20] which are very nearly unity between 2.8 and 4.0 eV and upon the expected dominance of interband transitions, which have unit quantum efficiency by definition, in the high-energy region. The general dependence of quantum efficiency on photon energy which we obtain is very similar to that reported by Weimer and Cope,[17] while magnitudes correspond more closely to those of Keck[18] and Fotland.[19].

The experimental results were interpreted by assuming that two independent absorption processes contributed significantly to the optical properties. One was attributed to a photoconductive process (superscript P) with an electron-hole pair quantum efficiency of unity in order to explain the high photon energy photoresponse while the second was attributed to a nonphotoconductive process (superscript N), whose quantum efficiency is zero, which accounted for the photo-

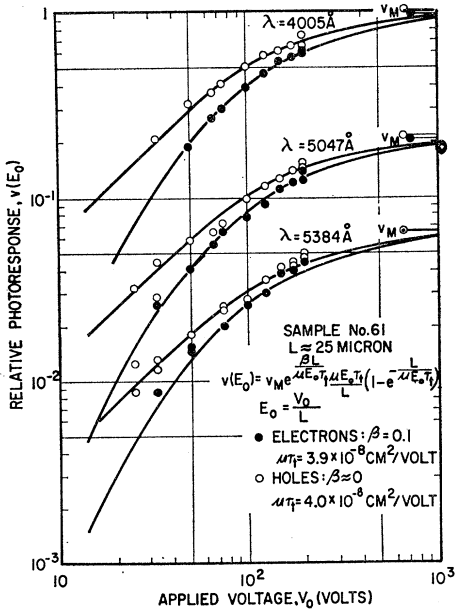

FIG. 3. Hecht curves typical of the experimental results.

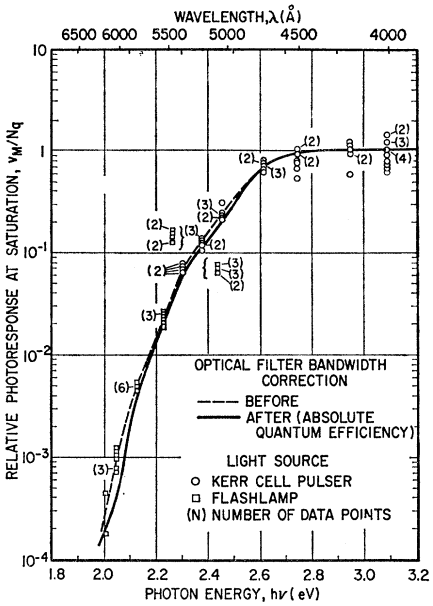

FIG. 4. Measured room-temperature quantum efficiency for vitreous selenium; normalized to unity at high photon energies.

response at low photon energies. Using this model, the measured quantum efficiencies and the known optical constants[28] of vitreous selenium (superscript S) were combined through Eq. (8) to give separately the imaginary parts of the dielectric constant appropriate to the (N) and (P) absorption processes.

$$\epsilon_2^N = (1-\eta)\,\epsilon_2^S \tag{10}$$

$$\epsilon_2^P = \eta\,\epsilon_2^S . \tag{11}$$

The results are shown in Fig. 5. The real parts of the dielectric constant were obtained using the dispersion relation[29] given in Eq. (2a). The parameter ϵ_2^N was assumed to be nonzero only in the energy region shown in Fig. 5, and for purposes of evaluation ϵ_2^P was given a value of zero for energies less than 1.5 eV. Since ϵ_2^S and ϵ_2^P are finite but unknown at energies above 5.17 eV, it was assumed that ϵ_2^S and ϵ_2^P were identical in this high energy region, allowing ϵ_1^P to be evaluated using the three known constants ϵ_1^S, ϵ_2^S, and ϵ_2^P in the energy region of interest:

$$\epsilon_1^P(\nu_0) = \epsilon_1^S(\nu_0) + \frac{2}{\pi}\int_0^{5.17\text{ eV}} \frac{[\epsilon_2^P(\nu)-\epsilon_2^S(\nu)](h\nu)\,d(h\nu)}{(h\nu)^2-(h\nu_0)^2} . \tag{12}$$

[28] Values for the ordinary index n between 1.5 and 5.1 eV and for the extinction coefficient k between 2.07 and 5.1 eV were taken from Ref. 11; the reflectivity values have been closely reproduced [D. Magde and J. L. Hartke (to be published)]. The extinction coefficient between 1.67 and 2.07 eV was taken from Ref. 8 and the values were reproduced by the authors (unpublished). The extinction coefficient in the 1.5- to 1.67-eV region was obtained from Ref. 12.

[29] The dispersion integral was evaluated at 46 points using the computer program of E. L. Kreiger, D. J. Olechna, and D. S. Story [General Electric Research Laboratory Report No. 63-RL-3458G, 1963 (unpublished)].

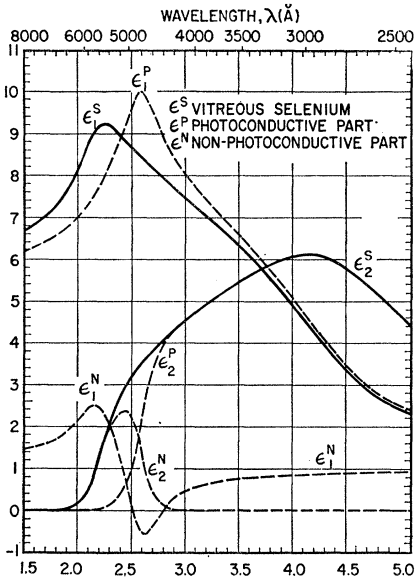

FIG. 5. Real and imaginary parts of the dielectric constant, ϵ_1 and ϵ_2, for vitreous selenium at room temperature and their resolved photoconductive and nonphotoconductive parts.

Values for absorption coefficients, shown in Fig. 6, were obtained from the parameters ϵ_1 and ϵ_2. It is clear that the sum of α^N and α^P does not equal α^S, the absorption coefficient of vitreous selenium, illustrating the statement of Sec. II that absorption coefficients are not additive. Instead, the low-energy (N) absorption is suppressed and the stronger high-energy (P) absorption is slightly enhanced when the two absorption mechanisms are combined. This suppression or enhancement is a result[30] of the ordinary index n^S being greater than n^N and slightly less than n^P and tends to smooth out any structure which might occur in the measured absorption coefficient α^S.

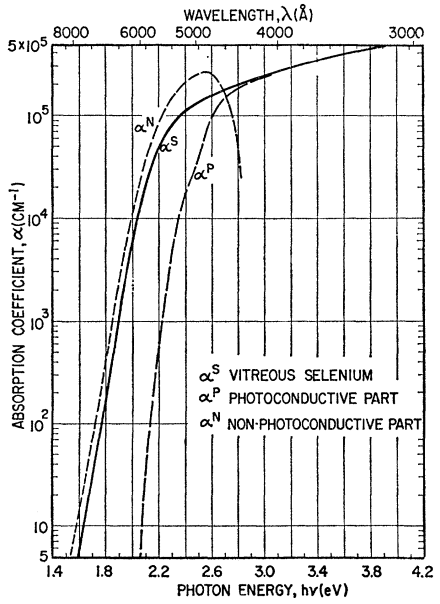

FIG. 6. Optical-absorption coefficient for vitreous selenium and its resolved photoconductive and nonphotonductive parts.

VI. DISCUSSION

The optical parameter ϵ_2^N obtained in the preceding section was found to be nearly Gaussian about its peak but had an exponential tail at lower energies. This is more clearly shown in Fig. 7, where the parameter $\epsilon_2^N(h\nu)^2$ is proportional to the normalized transition probability of Eq. (5b). Similar line shapes have been observed[31] only for excitons which were localized at an impurity center in an ionic crystal and have been explained[31] by an extension of Toyozawa's model[32] of

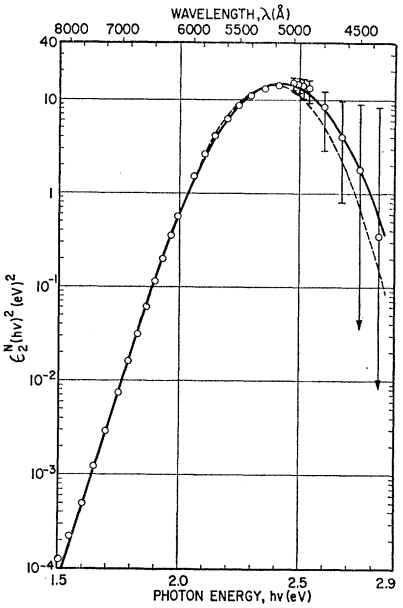

FIG. 7. Relative probability of nonphotoconductive transitions as fitted to the two-mode model of phonon-assisted exciton absorption. Dashed curve; approximate probability of Eq. (14a) with $A=3.5\times10^{-17}$ eV^2, $\sigma=18.5$ eV^{-1}, $\tau=4.99$ eV^{-1}, $h\nu_0=2.44$ eV. Solid curve; exact probability of Eq. (14b) with $A=8.3\times10^{-16}$ eV^2, $\sigma=16.7$ eV^{-1}, $\tau=4.50$ eV^{-1}, $h\nu_0=2.45$ eV.

phonon-assisted optical transitions which assumes that two different lattice modes are important configuration coordinates. One mode (e.g., longitudinal acoustic phonons) results in a near-linear dependence of the energy difference between excited and ground states on the configuration coordinate of this mode and is mainly responsible for the nearly Gaussian line shape near the absorption maximum. The other mode (e.g., longitudinal optical or transverse acoustic phonon) produces an energy difference which depends quadratically on the configuration coordinate for this mode and leads to the

[30] J. J. Hopfield, Phys. Rev. **112**, 1555 (1958).
[31] H. Mahr, Phys. Rev. **132**, 1880 (1963).
[32] Y. Toyozawa, Progr. Theoret. Phys. (Kyoto) **22**, 455 (1959); **20**, 53 (1958); Suppl. **12**, 111 (1959).

low energy exponential tail which may account for Urbach's empirical rule. The two-mode model of exciton absorption has recently been extended[33] to the case of intrinsic excitons which are momentarily self-trapped[34] through strong exciton-phonon coupling, placing the model in qualitative agreement with Urbach rule effects observed in a wide variety of ionic, compound, and organic semiconductors.

When broadened line absorption occurs, the delta function in Eq. (5b) is commonly replaced by a normalized shape factor $S(\nu)$, and the relative transition probability becomes

$$\epsilon_2\nu^2=(e^2h/2m)N_0\nu_0f_0S(\nu). \tag{13}$$

The relative transition probability as calculated by Mahr[31] for the two-phonon mode model of localized exciton absorption is

$$\epsilon_2(h\nu)^2=Ae^{\sigma h\nu}\int_\theta^\infty e^{-x^2}dx, \tag{14a}$$

where $\theta=\tau(h\nu-h\nu_0)+\sigma/2\tau$. The constant A contains the energy independent terms of Eq. (13) and the normalization constant of the shape factor. The resonant absorption frequency is ν_0 and the parameters τ and σ arise from the linear and quadratic modes, respectively. Published values[31] of $\sigma=21$ eV^{-1} and $\tau=5.7$ eV^{-1} for an ionic crystal at 300°K suggest that the expected absorption band would be quite broad with a half-width of several tenths of an electron volt and that the activation energy of the exponential tail would be of order kT. This model was applied to the shape of the nonphotoconductive (N) absorption and, as shown by the dashed curve of Fig. 7, resulted in a satisfactory fit except in the 2.45–2.55 eV range. Large uncertainties in the values of $\epsilon_2{}^N=(1-\eta)\epsilon_2$ resulted from the near unity values of the quantum efficiency when photon energy exceeded 2.6 eV. The limits of Eq. (14a) for large positive or negative values of θ differ by order $|\theta|^{1/2}$ from the limits obtained by Toyozawa,[33] suggesting that the fit to the absorption curve of Fig. 7 might be improved. This difference in limiting values arises from Mahr's omission of the pre-exponential factor $(h\nu_0-h\nu_l)^{-1/2}$ in Eq. (4) of Ref. 31 from his final convolution integral. The exact transition probability, which has also been calculated by McCumber,[35] obtained by including this factor is

$$\epsilon_2(h\nu)^2=Ae^{\sigma h\nu}\int_\theta^\infty \frac{e^{-x^2}dx}{(x-\theta)^{1/2}}. \tag{14b}$$

Evaluation of the integral is outlined in the Appendix. An interesting feature of Eq. (14b) is that its energy dependence in the exponential tail region is $\exp[(\sigma+0.4016\tau)h\nu]$ rather than the factor $\exp(\sigma h\nu)$ which results from Eq. (14a), necessitating a study of more than just the tail region to obtain σ when the Urbach effect is observed. The solid curve of Fig. 7 shows that the exact shape factor does give an improved fit to the (N) absorption, particularly in the high photon-energy region. Values used for the shape parameters σ and τ are remarkably near those obtained[31] for the localized exciton in KCl ($\sigma=21$ eV^{-1}, $\tau=5.71$ eV^{-1}).

When broadened line absorption occurs, additional information may be obtained by comparing the area under the weighted absorption curve to the integral[36,37] of Eq. (5b),

$$\int_0^\infty(\epsilon_2h\nu)d(h\nu)=(e^2h^2/2m)(E_l/E_0)^2N_0f, \tag{15}$$

where N_0 is the density of absorbing centers, f is their oscillator strength, and the additional factor E_l/E_0 is the ratio of the local electric field causing the transition to the macroscopic field. The field correction term[38] takes into account the perturbation introduced by the localized center and may vary between $E_l/E_0=(n^2+2)/3$ for tightly-bound or very localized wave functions (the Lorentz correction) and unity for weakly-bound or diffuse states. Using Eq. (15) and the solid curve of Fig. (7), a value of $(E_l/E_0)^2N_0f=1.1\times10^{21}$ cm^{-3} was obtained. By employing the known bounds $f\leq1$ and $N_0\leq3.3\times10^{22}$ cm^{-3} (the atomic density of vitreous selenium) and the local field correction limits of $(E_l/E_0)^2=13.4$ (the Lorentz correction with $n=3$) and unity, the resuls of Table I are obtained which clearly outline the ranges of the parameters N_0 and f. These results will be discussed later in this section.

Our assignment of the nonphotoconductive (N) absorption is plausible. The strong absorption band, its width, and its shape are consistent with the absence of photoconductivity since the mechanism used to explain this band requires strong coupling between phonons and the localized exciton, the strength of this coupling causing a self-trapped level to branch off from

TABLE I. Possible densities N_0 and oscillator strengths f of the nonphotoconducting absorption centers in vitreous selenium.

Assumed constant	Local field correction $(E_l/E_0)^2$	N_0(cm^{-3})	f
N_0 atomic	13.4	3.3×10^{22}	2.4×10^{-3}
N_0 density	1.0	3.3×10^{22}	3.3×10^{-2}
N_0 unit cell	13.4	1.1×10^{22}	7.3×10^{-3}
N_0 density	1.0	1.1×10^{22}	9.8×10^{-2}
f	1.0	1.1×10^{21}	1
f	13.4	8.2×10^{19}	1

[33] Y. Toyozawa, Tech. Report of the Inst. for Solid State Physics (Univ. of Tokyo) Ser. A, No. 119 (1964).
[34] Ref. 16, p. 181.
[35] D. E. McCumber, Phys. Rev. **135**, A1676 (1964).
[36] D. L. Dexter, Phys. Rev. **101**, 48 (1956).
[37] Separate papers by M. Lax and C. Herring, *Proceedings of the Conference on Photoconductivity, Atlantic City, November 4–6, 1954*, edited by R. G. Breckenridge *et al.* (John Wiley & Sons, Inc., New York, 1956).
[38] D. L. Dexter in *Solid State Physics*, edited by F. Seitz and D. Turnbull (Academic Press Inc., New York, 1958), Vol. 6.

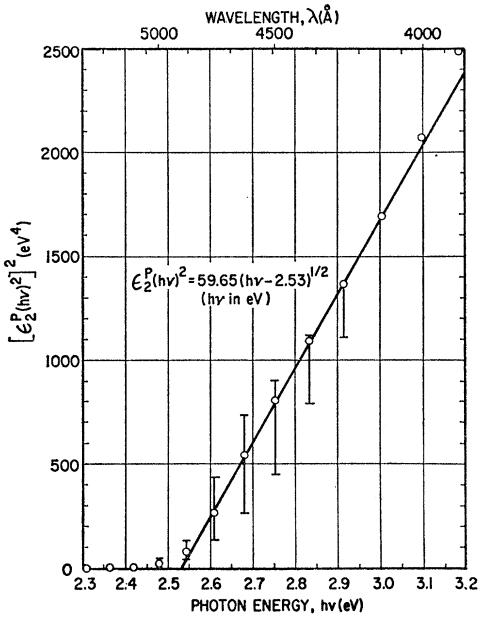

FIG. 8. Relative probability of photoconductive transitions as fitted to the model of direct, allowed interband transitions.

the intrinsic exciton band. The localized excited state is expected[34] to decay nonradiatively by multiple phonon emission.

Since interband transitions were expected for the (P) absorption, attempts were made to obtain a linear relation between $[\epsilon_2{}^P(h\nu)^2]^m$ and photon energy for m values between $\frac{1}{3}$ and 2. This range includes all m values expected for simple direct or indirect, allowed or forbidden interband transitions. As shown in Fig. 8, a good fit was obtained between 2.6 and 3.0 eV using $m=2$, indicating that optical absorption at these energies which produces photoconductivity may be attributed to direct, allowed interband transitions. Values for m of 1, $\frac{2}{3}$, $\frac{1}{2}$, or $\frac{1}{3}$ led to rather poor fits which were valid over a photon energy range of, at most, 0.15 eV. Deviations from the straight line of Fig. 8 at high photon energies are probably caused by increases in the effective densities of states (decreases in band curvature) although the onset of new transitions would give a similar increase. The probability of direct, allowed transitions between nondegenerate, parabolic valence and conduction bands is proportional to[39]

$$\epsilon_2(h\nu)^2 = (e^2\hbar^2/m)(2m_r/\hbar^2)^{3/2}E_g f_{vc}(h\nu - E_g)^{1/2}, \quad (16)$$

where m_r is the reduced density-of-states effective mass ($m_r^{-1}=m_e^{-1}+m_h^{-1}$), E_g is the band gap, and f_{vc} is the oscillator strength for dipole transitions which is given by Eq. (6) with $\exp(i\mathbf{q}\cdot\mathbf{r})$ approximated by unity. According to Eq. (16), the constants associated with the data fitting of Fig. 8 indicate a band gap of 2.53 eV and a value of 1.6 for the parameter $(m_r/m)^{3/2}f_{vc}$.

By subtracting the resonance energy of the exciton absorption, $h\nu_0=2.45$ eV, from the band-gap energy, an exciton binding energy of 0.08 eV is obtained. The binding energy of a Wannier, or weakly-bound, exciton may be calculated using a hydrogenic model modified by the static dielectric constant ϵ_0 and the reduced effective mass m_r of the hole-electron pair. Assuming that the observed transitions are to the lowest excited state ($n=1$ in the hydrogenic series), the binding energy is

$$E_B = 13.6\epsilon_0^{-2}(m_r/m)\ \text{eV}. \quad (17)$$

A value of $m_r=0.23m$ is obtained using the above binding energy and a static dielectric constant of 6.0, which give an exciton radius β of

$$\beta = \epsilon_0 a_0(m/m_r) = 26a_0, \quad (18)$$

where a_0 is the Bohr radius. This exciton radius of 13 Å is sufficiently large to justify using the Wannier model. The oscillator strength for direct transitions to the lowest excited state of a Wannier exciton has been estimated[40] to be (lattice constant/exciton radius) cubed times the oscillator strength of interband transitions, the latter factor being of order unity if the transitions are direct and allowed. Three lowest-lying conduction bands and three uppermost valence bands are expected for vitreous selenium since the spiral chain structure, just like the hexagonal lattice, has three atoms per unit cell. If these bands are degenerate, the f value as estimated above is 1.4×10^{-2}, using a mean lattice constant of 3.1 Å obtained from the inverse cube of the atomic density. This oscillator strength compares favorably with the value of 3.3×10^{-2} given in Table I for one absorbing center per atom and for a local field correction of unity which is expected if the exciton radius is large compared to the interatomic distance. If the triple bands are nondegenerate, one conduction and one valence band might dominate the optical transitions, and the unit-cell density, $N_0=1.1\times10^{22}$ cm^{-3}, becomes the density of absorbing centers. An oscillator strength of 9.8×10^{-2} is then obtained from Table I, again using $E_l/E_0=1$, and remains in agreement with the estimated value of 5.1×10^{-2} which is now obtained by substituting the unit-cell volume for the cube of the lattice constant.

Assignment of the nonphotoconductive absorption to intrinsic excitons is consistent with optical absorption observed[13] in hexagonal selenium where a peak occurs at the absorption edge for light polarized normal to the c axis. This peak suggests the presence of exciton absorption in the crystalline solid although the structure has been attributed by Gobrecht and Tausend[13] to valence-band splitting.

The reduced effective mass $m_r=0.23m$ obtained from the exciton binding energy, when combined with the result $(m_r/m)^{3/2}f_{vc}=1.6$ obtained from the photo-

[39] T. P. McLean in *Progress in Semiconductors*, edited by A. F. Gibson *et al.* (John Wiley & Sons, Inc., New York, 1961), Vol. 5.

[40] G. Dresselhaus, Phys. Rev. **106**, 76 (1957); R. J. Elliott, Phys. Rev. **108**, 1384 (1957).

conductive transitions, gives the one-electron value $f_{vc}=15$ which is, of course, unrealistic and which we explain as follows: The sum rule[41] for direct, allowed interband transitions is

$$\sum_{c'} f_{vc'} = 1+(m/m_v), \tag{19}$$

where the sum is carried out over all conduction bands; thus oscillator strengths of order unity are expected when valence-band effective masses are of order unity. The probable cause of the discrepancy between the above oscillator strength of 15 and the near-unity expected value lies in the expected multiple band structure of selenium. If two or more valence bands are degenerate or nearly degenerate, the heavy-hole band will tend to dominate the interband transitions because of its greater density of states, while the broad exciton absorption will probably include transitions from several valence bands. An equivalent argument holds for the conduction bands. The exciton binding energy could then contain appropriate averages over the effective masses of the bands while the reduced density-of-states effective mass which applies to interband transitions would be of order unity, giving a more reasonable oscillator strength of $f_{vc}\approx 1$–2, and would mainly depend on the effective masses of the heavy bands which have the least curvature. Anisotropic bands would also complicate the interpretations as would random orientation of the unit cell in the vitreous solid.

Direct allowed interband transitions have accounted for a portion of the photoconductive absorption, but Fig. 9 shows that this model fails to explain the absorption in the 2.0- to 2.5-eV region. Drift mobility measurements[1,4] have suggested that levels are present in vitreous selenium which extend 0.14 eV above the valence band and 0.28 eV below the conduction band. These levels act as shallow traps for macroscopic charge transport by exchanging carriers with their nearby bands and are thought to arise from the noncrystalline nature of the solid. Since the quantum-efficiency measurements reported here were accomplished by observing macroscopic charge transport, optical transitions to or from these shallow traps would lead to photoconductivity, even though optically generated carriers were initially immobile, because of the immeasurably short lifetimes for thermal freeing of the trapped carriers. Thresholds as measured from the band gap are shown in Fig. 9 for these band-trap and trap-trap photoconductive transitions and qualitatively account for the (P) absorption edge which has a slight amount of curvature near the thresholds. The absence of sharp structure between 2.0 and 2.5 eV indicates that these traps are not energetically discrete levels but rather that they are distributed continuously

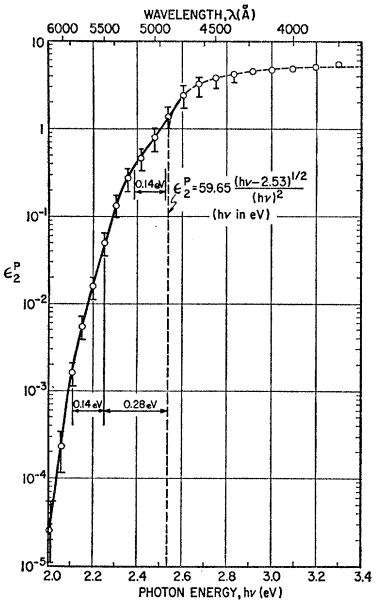

FIG. 9. Imaginary part of the dielectric constant for photoconductive transitions indicating the effect of shallow traps or band tails in the low-photon-energy region.

in energy between the bands edges and the 0.14- and 0.28-eV limits.

Our treatment has considered only transitions to the lowest exciton state and has neglected all higher bound states as well as the exciton continuum, even though transitions to the continuum states should produce significant and energy independent absorption[39] at photon energies equal to or slightly greater than the band gap energy. The absence of such absorption in our results probably arises from the noncrystalline nature of vitreous selenium. The radii of bound exciton states increase as the square of the radial quantum number while the radius of the $n=1$ state was estimated to be 13 Å, suggesting that radii of all other excited states are greater than the spatial extent of short-range order. For such a case the electron-hole Coulomb interaction may not be sufficiently strong to justify the use of the exciton concept. Similar effects have been observed[42] for solid Kr and Xe in which absorption by Wannier excitons involved only the lowest excited state when defects were present in unannealed crystals.

VII. SUMMARY

The imaginary part of the dielectric constant has been shown to be the most useful additive optical parameter when several absorption mechanisms are important, and the measurable quantum efficiency has been related to appropriately weighted components of ϵ_2. By using this relation with the experimentally observed quantum efficiency and the known optical parameters of vitreous selenium, a band model has been developed which is consistent with the optical, photoconductive, and charge transport properties of this noncrystalline semiconductor. Nonphotoconduc-

[41] F. Seitz, *Modern Theory of Solids* (McGraw-Hill Book Company, Inc., New York, 1940), p. 652; J. Bardeen, F. J. Blatt and L. N. Hall, *Proceedings of the Conference on Photoconductivity, Atlantic City, November 4–6, 1954*, edited by R. G. Breckenridge *et al.* (John Wiley & Sons, Inc., New York, 1965).

[42] G. Baldini, Phys. Rev. **128**, 1562 (1962).

tive absorption near the edge is attributed to transitions into an intrinsic exciton state lying 0.08 eV below the conduction band which is rapidly self-trapped. Localization of this exciton through strong interaction with two lattice modes appears to be consistent both with the shape of the absorption band and with the negligible thermal disassociation probability of the bound hole-electron pair. The reduced effective mass of the exciton is estimated to be 0.23 free-electron masses. Absorption which produces one mobile electron and one mobile hole per absorbed photon is interpreted in terms of direct, allowed optical transitions between extremes of the valence and conduction bands which are separated by 2.53 eV. The reduced effective mass for interband transitions is thought to be of order unity, differing from the reduced exciton mass as a result of degenerate or nearly degenerate bands as well as possible band anisotropies and random orientations of the unit cell in this solid which has short-range but not long-range atomic order.

Photoconductive absorption occurring on the low-energy side of the band gap is assigned to states in the otherwise forbidden gap which are energetically near the band edges and which act as shallow traps for macroscopic charge transport. The absence of strong structure in this absorption supports an earlier suggestion[4] that the shallow levels are tails of the conduction and valence bands produced by long-range disorder. Optical absorption associated with these states tends to obscure structure at the absorption edge produced by the exciton, although structure should be observable in crystalline selenium since the band tails would then be absent. A peak superimposed on the absorption edge of hexagonal selenium has been observed[13] for light polarized normal to the c axis, while the edge for parallel polarization is broad and structureless just as for vitreous selenium. Both edges for the crystal may be caused by exciton absorption although photoconductivity at the absorption edge has been reported.[43] If the exciton model is applicable to hexagonal selenium, its band gap would be 2.3–2.4 eV, very near that of the vitreous allotrope and greater than earlier estimates.[13,43]

Interpretation of the absorption edge in vitreous selenium in terms of exciton absorption differs from earlier models[2,5] based on optical transitions between localized states and one band, and is necessitated by the measurement of hole-electron pair generation near the absorption edge. Generation of electrons alone by 1.2- to 1.85-eV photons, as reported in Sec. IV, confirms the suggestion[5] that electrons may be excited from trapping states just below the Fermi level to the conduction band, but these transitions are not responsible for the absorption edge since the quantum efficiency for this process is very small, indicating that absorption in the 1.2- to 1.85-eV range is primarily due to a nonphotoconductive process. The results of careful optical-absorption and quantum-efficiency measurements should be related to the densities of these deep traps which have been estimated by space-charge-limited-current measurements.[2–5]

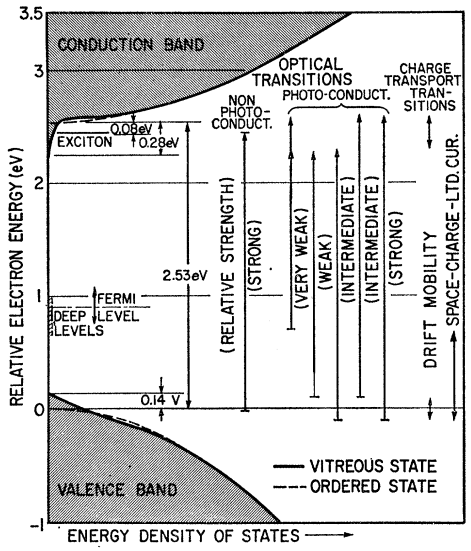

FIG. 10. Electronic states in vitreous selenium at room temperature as indicated by optical, photoconductivity, and charge-transport measurements.

A summary of the electronic states used here and elsewhere to explain the optical, photoconductive, and charge-transport properties of vitreous selenium is given in Fig. 10. Only the exciton level is new, the other states in the band gap having been introduced to explain the results of transport measurements.[1–5] One should note that the optical band gap of 2.53 eV as interpreted here is actually a fictitious parameter, being the distance between extrapolated rather than real zeros in the densities-of-states curves. Although well-defined band edges are expected for crystalline solids, they might be better defined as regions of transition from conducting to nonconducting states in a vitreous solid.

Quantitative application of the band model to vitreous selenium has given parameters which must be regarded with caution. In particular, the reduced effective masses of order unity probably result from rather complicated averages over orientation and band index. Faraday rotation measurements[44] have given effective masses of order ten in both vitreous and hexagonal selenium, but these also should be accepted with some reservation since the wavelength ranges of the measurements were somewhat limited and the results were interpreted using either single-harmonic-oscillator (bound-electron) or free-carrier-absorption models.

[43] V. Prosser, Czech. J. Phys. **B10**, 306 (1960).

[44] H. Gobrecht, A. Tausend, and I. Bach, Z. Physik **166**, 76 (1962); H. Gobrecht, A. Tausend, and J. Hertel, Z. Physik **178**, 19 (1964).

The band model proposed here for vitreous selenium may be tested in a number of ways. One very appropriate measurement would be to observe the Faraday rotation near the absorption edge, since exciton absorption should be manifested as weak structure superimposed on the strong structure arising from interband transitions. Exciton effects should be more pronounced at low temperatures since the exciton absorption band is expected to sharpen and to reach a higher peak value as temperature decreases, suggesting that some structure might then be observed in the optical reflectance and absorption spectra. Similar measurements of the optical properties and quantum efficiencies of hexagonal selenium for a complete set of crystal orientations with respect to the polarization and Poynting vectors of the incident light would likewise be instructive.

The method demonstrated here which quantitatively resolves photoconductive and nonphotoconductive optical-absorption processes is a useful tool. One valuable application of this technique would be to test the proposal[33] that absorption edges of solids which obey Urbach's rule are caused by two-mode phonon-assisted transitions to exciton states which are localized either at defects or by self-trapping. For either case one might expect decay of the exciton rather than thermal dissociation and thus nonphotoconductive absorption by the exciton.

ACKNOWLEDGMENTS

The authors are grateful to R. S. Knox for his many instructive comments and encouragement. Many of the measurements were made by R. L. Lozen and G. F. Meister. All samples were prepared by J. K. Johnson. Computer calculations were carried out by Andrew Wilson and were facilitated by the advice of D. J. Olechna. A number of hand calculations were made by R. A. Bell.

APPENDIX: EVALUATION OF THE EXACT SHAPE-FUNCTION INTEGRAL

A solution in closed form does not exist for the integral contained in Eq. (14b):

$$\mathrm{I}(\theta)\equiv\int_{\theta}^{\infty}\frac{e^{-x^2}dx}{(x-\theta)^{1/2}}. \tag{A1}$$

Numerical evaluation is facilitated by making the substitution $y=(x-\theta)^{1/2}$ which results in the more tractable integral

$$\mathrm{I}(\theta)=2\int_{0}^{\infty}e^{-(y^2+\theta)^2}dy. \tag{A2}$$

TABLE II. The integral $\mathrm{I}(\theta)$.

θ	$\mathrm{I}(\theta)$	θ	$\mathrm{I}(\theta)$	θ	$\mathrm{I}(\theta)$
−2.50	1.164	−1.00	1.974	+1.25	2.164×10^{-1}
−2.25	1.242	−0.75	2.108	+1.50	1.014×10^{-1}
−2.00	1.340	−0.50	2.150	+1.75	4.220×10^{-2}
−1.75	1.465	+0.50	1.066	+2.00	1.561×10^{-2}
−1.50	1.619	+0.75	6.998×10^{-1}	+2.25	5.122×10^{-3}
−1.25	1.796	+1.00	4.118×10^{-1}	+2.50	1.490×10^{-3}

Table II lists the results of numerical integrations made by a computer.

Several useful infinite series exist for the integral. When the parameter θ is large and positive the term $\exp(-y^4)$ in the integrand of Eq. (A2) may be expanded in a power series and the result may be integrated term by term to give the following convergent series:

$$\mathrm{I}(\theta)=\left(\frac{\pi}{2\theta}\right)^{1/2}e^{-\theta^2}\sum_{n=0}^{\infty}\frac{(-1)^n(4n)!}{n!(2n)!2^{6n}\theta^{2n}}. \tag{A3}$$

The first six terms of the series give accurate results when the inequality $\theta\geq2.5$ holds. In the region $|\theta|<0.8$, the substitution $Z=(x-\theta)^2$ is made in Eq. (A1) and all factors containing θ are expanded in a power series. After term-by-term integration, the following series is obtained:

$$\mathrm{I}(\theta)=\tfrac{1}{2}\Gamma(\tfrac{1}{4})\left(1-\frac{\theta^2}{2!}+\frac{5\theta^4}{4!}-\frac{5\times9\theta^6}{6!}+\frac{5\times9\times13\theta^8}{8!}-\cdots\right)-\theta\Gamma(\tfrac{3}{4})\left(1-\frac{3\theta^2}{3!}+\frac{3\times7\theta^4}{5!}-\frac{3\times7\times11\theta^6}{7!}+\cdots\right). \tag{A4}$$

Values for the gamma functions are $\frac{1}{2}\Gamma(\frac{1}{4})=1.8128$ and $\Gamma(\frac{3}{4})=1.2254$.

A convergent series expansion was not found for the region where θ is large and negative. The following series, which contains selected terms of a divergent expansion, does represent the integral $I(\theta)$ to within $\frac{1}{2}\%$ for $-\theta>2$:

$$\mathrm{I}(\theta)=\left(-\frac{\pi}{\theta}\right)^{1/2}\left[\frac{1+\mathrm{erf}(-\theta)}{2}\right]\sum_{n=0}^{5}\frac{(4n)!}{n!(2n)!2^{6n}\theta^{2n}}. \tag{A5}$$

A more useful relation follows which was empirically determined and which is accurate to $\frac{1}{2}\%$ in the range $-2.0<\theta<-0.9$:

$$\mathrm{I}(\theta)=2.957\exp(0.4016\theta). \tag{A6}$$